Available online at www.sciencedirect.com
SCIENCE DIRECT
Journal of Solid State Chemistry 179 (2006) 1041–1052
JOURNAL OF SOLID STATE CHEMISTRY
www.elsevier.com/locate/jssc

Directional metal–hydrogen bonding in interstitial hydrides. III. Structural study of $ErCo_3D_x$ ($0 \leqslant x \leqslant 4.3$)

Y.E. Filinchuk, K. Yvon*

Laboratoire de Cristallographie, Université de Genève, 24 quai E. Ansermet, CH-1211 Genève 4, Switzerland

Received 27 October 2005; received in revised form 22 December 2005; accepted 1 January 2006
Available online 3 February 2006

Abstract

The $ErCo_3$–D_2 system has been studied by in situ neutron powder diffraction (NPD) at 60 °C and 0–16 bar deuterium pressure. Two deuteride phases were identified, β-$ErCo_3D_{1.07-1.38}$ and γ-$ErCo_3D_{3.7-4.3}$. They were structurally characterized at the compositions β-$ErCo_3D_{1.37}$ and γ-$ErCo_3D_{3.7}$ by high-resolution neutron and synchrotron powder diffraction. In contrast to the analogous nickel systems RNi_3–D_2 (R = Er, Ho; see part I, J. Alloys and Compds. 404–406 (2005) 89–94, and part II, J. Alloys and Compds. 2005, in press), their structures preserve the symmetry of the parent alloy ($PuNi_3$-type, space group R-3m). Deuterium occupies mainly AB_2 building blocks in the β-phase, and AB_2 and AB_5 building blocks in the γ-phase. In the AB_2 building blocks cobalt is surrounded by an average of 3.8 (β-$ErCo_3D_{1.37}$) and 4.4 D-atoms (γ-$ErCo_3D_{3.7}$) in disordered distorted octahedral configurations (point symmetry −3), in contrast to nickel that is surrounded by ~3 (β_1- and β_2-RNi_3D_x, R = Er, Ho) and ~4 (γ-$ErNi_3D_{3.7}$) D-atoms in disordered trigonal (pyramidal) and tetrahedral configurations, respectively (point symmetry 3). These results indicate that the D-atom distributions in this homologous series depend on the nature of the transition element rather than on geometric factors, and that directional bonding effects similar to those in non-metallic complex transition metal hydrides also prevail in metallic interstitial metal hydrides.

Keywords: Hydrogen storage materials; Crystal structure and symmetry; Neutron diffraction

1. Introduction

In the first two papers of this series directional metal–hydrogen bonding effects have been investigated by neutron powder diffraction (NPD) on the two nickel based systems RNi_3D_x (R = Er [1], Ho [2]). Both crystallize with $PuNi_3$-type metal structures and contain three deuteride phases having the approximate compositions x~1.3 (β_1), x~2 (β_2) and x~3.8 (γ), in which deuterium occupies mainly AB_2-type building blocks in the β-phase, and AB_2 and AB_5-type building blocks in the γ-phase (for structure drawings see [3]). The structure data obtained so far are summarized in Table 1. In the AB_2-type building blocks nickel is surrounded by ~3 (β_1- and β_2-RNi_3D_x, R = Er, Ho) and ~4 (γ-$ErNi_3D_{3.7}$) D-atoms in disordered trigonal (pyramidal) and tetrahedral configurations, respectively. Furthermore, in contrast to the centrosymmetric alloys (space group R-3m) the deuterides lack inversion symmetry (space group R-3m). Structure data on analogous cobalt-based RCo_3D_x systems (R = rare earth) have so far only been reported for R = Er [4–6]. Cell parameters are known for β- and γ-$ErCo_3H_x$ hydrides [4,5], while D-atom positions for γ-$ErCo_3D_{4.1}$ have been reported from NPD data at 300 K [6]. Interestingly, cobalt in the AB_2-type building blocks was found to be surrounded by ~4 D-atoms in a disordered octahedral rather than tetrahedral configuration. Three partially occupied deuterium atom sites were found, yielding an overall D content of 3.4 D-atoms per formula unit (f.u.). The discrepancy between the measured and refined D content is presumably due to the limited quality of the NPD data that did not allow all possible D sites in the structure to be identified. Very recently, NPD data on the analogous yttrium system YCo_3D_x [7] suggested the existence of three deuteride phases at compositions similar to those in the nickel systems, i.e., x~1.3 (β_1), x~2 (β_2) and x~4.6 (γ). However, their structural symmetry and

*Corresponding author. Fax: +41 22 379 6864.
E-mail address: klaus.yvon@cryst.unige.ch (K. Yvon).

0022-4596/$ - see front matter © 2006 Elsevier Inc. All rights reserved.
doi:10.1016/j.jssc.2006.01.001

transition metal (T) environments differed significantly from those in the nickel systems, in the sense that the deuterides preserved inversion symmetry and cobalt in the AB_2-type building blocks was surrounded by 4–6 D-atoms in disordered, distorted octahedral configurations [7]. These results are in line with the expected role of T elements for directional metal–hydrogen bonding in "interstitial" metal hydrides as suggested for the nickel-based systems RNi_3D_x (R = Er [1], Ho [2]). In order to obtain further evidence for this view, it was decided to reinvestigate the cobalt-based system $ErCo_3$–H_2. This system is particularly suitable because it has been investigated in detail before with respect to both composition and thermodynamic properties. Measurements of pressure-composition isotherms (PCT), for example, confirmed the existence of two hydride phases, a β-phase extending from $x = 1.15$ to 1.65, and a γ-phase extending from $x = 3.55$ to at least 4.15, and enthalpies of hydrogen absorption were derived for both phases [8]. Rates of hydrogen absorption of $ErCo_3$ have been reported to temperatures down to −196 °C [9] and rates of hydrogen desorption from β- and γ-$ErCo_3H_x$ were measured to temperatures up to 120 °C [10].

In this paper, we report new structure data on γ-$ErCo_3D_x$ as obtained by high-resolution neutron and synchrotron powder diffraction, and for the first time also on β-$ErCo_3D_x$. Furthermore, in situ NPD experiments were performed in order to study the absorption behaviour of $ErCo_3D_x$ at 60 °C. A comparison between the known RT_3D_x (T = Co, Ni) systems shows that they differ in a characteristic way with respect to the local deuterium environment of the transition element.

2. Experimental

2.1. Synthesis and preliminary X-ray diffraction experiments

Four samples of nominal composition $ErCo_3$, one of 3 g and three of 6 g mass, were prepared by arc melting pieces of erbium (99.9%, redistilled, Johnson Matthey) and cobalt (99.9+%, Alfa) under argon atmosphere. No significant weight losses occurred during melting. The ingots were not annealed, since $ErCo_3$ forms congruently from the melt. X-ray powder diffraction (Co $K\alpha$ radiation) showed that the alloys were well crystallized and consisted of nearly pure $ErCo_3$ phase with not more than ~1% of Er_2O_3 impurity phase. The cell parameters for the $ErCo_3$ phase (space group R-3m, $PuNi_3$ structure type) as found in the various samples are:

1. $a = 4.9778(4)$, $c = 24.239(2)$ Å, $V = 520.15(7)$ Å^3;
2. $a = 4.9778(1)$, $c = 24.2443(5)$ Å, $V = 520.24(2)$ Å^3;
3. $a = 4.9781(1)$, $c = 24.2459(9)$ Å, $V = 520.34(3)$ Å^3;
4. $a = 4.9797(4)$, $c = 24.251(2)$ Å, $V = 520.78(7)$ Å^3, c/a~4.87.

Atomic coordinates as derived by Rietveld refinement of the diffraction pattern of sample No. 3 are given in Table 2.

Deuteration (D_2 gas, 99.8%, AGA) was carried out in autoclaves after performing one or two activation cycles at 80 °C between 80 bar D_2 pressure (absorption) and vacuum (desorption). Samples containing the β-$ErCo_3D_x$ deuteride were obtained by exposing the alloys Nos. 1 and 2 to a constant deuterium pressure of 1.8 bar at 80 °C for 1

Table 1
Nickel and cobalt-based deuterides with $PuNi_3$-type metal structure, and the average D atom configurations around their Ni and Co sites in the AB_2 building blocks as determined from previous neutron powder diffraction works

RNi_3D_x	Space group	Average D atom configuration at Ni	RCo_3D_x	Space group	Average D atom configuration at Co
β_1-$ErNi_3D_{1.23}$ [1]	$R3m$	Trigonal pyr. (2.8)	β_1-$YCo_3D_{1.24}$ [6]	R-3m	Octahedral (4.0)
β_2-$ErNi_3D_{1.97}$ [1]	$R3m$	Trigonal pyr. (~3)	β_2-$YCo_3D_{2.0}$ [6]	R-3m	Octahedral (6.0)
γ-$ErNi_3D_{3.75}$ [1]	$R3m$	Tetrahedral (~4)	γ-$YCo_3D_{4.6}$ [6]	R-3m	Octahedral (6.0)
β_1-$HoNi_3D_{1.3}$ [2]	$R3m$	Trigonal pyr. (2.9)	γ-$ErCo_3D_{3.4}$ [5]	R-3m	Octahedral (4.2)
β_2-$HoNi_3D_{1.8}$ [2]	$R3m$	Trigonal pyr. (3.0)			

Table 2
Atomic coordinates and thermal parameters of $ErCo_3$ (sample No. 3) from X-ray powder diffraction[a]

Atom	Wyckoff site	x	y	z	U_{iso}, Å^2
Er1	3a	0	0	0	0.0021(6)
Er2	6c	0	0	0.14016(7)	0.0021(6)
Co1	3b	0	0	1/2	0.0059(8)
Co2	6c	0	0	0.33340(17)	0.0059(8)
Co3	18h	0.5030(4)	$-x$	0.08106(10)	0.0059(8)

[a] $R_B = 0.049$, $R_F = 0.054$, $\chi^2 = 2.26$, $R_p = 0.027$, $R_{wp} = 0.035$ (not corrected for background), 143 "independent" reflections, 58 "effective" (accounting resolution [11]) reflections.

day, then decreasing the temperature to 50 °C and setting the pressure to 1.1 bar for 8 h. The autoclaves were quenched in cold water and then opened in air, and the samples were filled into vanadium cans that were tightly sealed. Samples containing the γ-$ErCo_3D_x$ deuteride were prepared by exposing the alloys Nos. 3 and 4 to a constant deuterium pressure of 20 bar at 80 °C for 1 day. The autoclaves were slowly cooled to room temperature and then opened in air, and the samples were rapidly filled into vanadium cans and sealed to prevent deuterium desorption. All reaction products were black powders that could be handled in air without detectable oxide formation. Each sample consisted of a single deuteride phase that desorbed slowly deuterium if not tightly sealed. Samples 1 and 3 were studied by synchrotron powder diffraction and samples 2 and 4 by NPD. As shown below, the cell parameters of the corresponding phases as obtained by these two techniques were highly reproducible.

2.2. Structure characterization by synchrotron and NPD

For the synchrotron experiments, samples 1 and 3 were filled into thin-walled glass capillaries immediately before data collection. Sample 3 containing the relatively deuterium rich γ-$ErCo_3D_x$ was freshly charged with 20 bar of deuterium and the pressure released only 5 min before the diffraction experiment. Powder patterns were collected at a Swiss–Norwegian beamline at ESRF (Grenoble) by using the wavelengths $\lambda = 0.52014(1)$ Å (β-phase) or 0.50014(1) Å (γ-phase), Debye–Scherrer geometry, 2θ range 4.0–38.5° with step size 0.005° (β-phase) or 3.0–43.5° with step size 0.004° (γ-phase). The wavelengths and zero-shifts were refined from a standard Si sample. Neutron powder patterns were collected on samples 2 and 4 at the diffractometer HRPT at SINQ (PSI; Villigen) at the wavelenghts $\lambda = 1.49418(2)$ Å (β-phase) or 1.49381(1) Å (γ-phase), 2θ range 4.5–164.5° step size 0.1°, data collection time ~7 h per pattern. The wavelengths and zero-shifts were refined from the measurements of a standard $Na_2Ca_3Al_2F_{14}$ (NAC) sample.

The structures were refined in centrosymmetric space group $R\bar{3}m$ by using the Fullprof Suite [11]. No evidence for lattice distortions of the β- or γ-phase deuterides was found from the synchrotron data. As a starting model the atomic parameters of γ-$ErNi_3D_{3.75}$ as described in $R\bar{3}m$ [1] and the cell and profile parameters as derived from a profile fitting of the respective NPD patterns were used. For β-$ErCo_3D_x$ only two out of six deuterium positions showed non-zero occupancies (D1, D2) and thus were retained in subsequent structure refinements. For γ-$ErCo_3D_x$ five deuterium atom positions (D1, D3–D6) were found to be occupied, while one (D2) was empty. Difference Fourier maps were analysed for the possible presence of other D atom sites. Refinements in non-centrosymmetric space group $R3m$ showed no evidence for preferential D atom order and did not improve the quality of the fit.

Structure refinements for the β- and γ-$ErCo_3D_x$ deuterides were done independently on synchrotron and neutron diffraction data. In each case, all positional parameters were refined by considering anisotropic thermal displacements for Er1, Er2, Co1 and Co2 (2 refined parameters per site, $U_{22} = U_{11}$, $U_{12} = 1/2U_{11}$, $U_{13} = U_{23} = 0$), isotropic displacements for Co_3, and an overall isotropic displacement parameter for all D-atom sites. While the occupancies of the metal sites were close to unity and thus fixed at 100%, those of the D-atom sites were smaller than unity and thus refined. In addition to the structural parameters listed above, 2 cell parameters and 2 parameters accounting for a peak asymmetry were refined. A pseudo-Voigt profile was used along with a hexagonal strain model to account for a little anisotropic peak broadening. One parameter was introduced to correct for minor preferred orientation along [001]. The background was described by a Fourier filtered polynomial function. The cubic Er_2O_3 impurity phase (~1%) was included into the refinement when necessary. Refinement results are listed in Table 3, and the observed, calculated and difference patterns are presented in Figs. 1 and 2.

2.3. In situ NPD

The phase transitions in the $ErCo_3$–D_2 system upon deuterium absorption were monitored by loading a 6 g sample of γ-$ErCo_3D_x$ into a steel container which was placed into a furnace installed at the neutron powder diffractometer DMC at SINQ (PSI, Villigen). The system was connected to a deuteration equipment available at PSI and evacuated at 87 °C until complete deuterium desorption. The temperature was then fixed at 60 °C during the entire in situ diffraction experiment. The first powder pattern showed that the deuteride had transformed into the pure deuterium-free $ErCo_3$ alloy. Deuterium gas was then added by small portions at various pressures (see Table 4). The first portion was immediately absorbed by the sample, leading to an increase of the sample temperature by ~10 °C within a few seconds. After adding another portion of D_2 gas the system was kept at 60 °C for 30 min to reach thermal equilibrium, and a diffraction pattern was collected during 3 h at $\lambda = 2.5687$ Å in Debye–Scherrer geometry within the 2θ range 15–100° (step size 0.1°). The pressure was increased in small steps up to a maximum of 16 bar, and diffraction patterns were collected at each step after the sample had reached thermal equilibrium. The last pattern was collected after cooling the sample to 25 °C under 16 bar of deuterium pressure, yielding the most deuterium-rich γ-$ErCo_3D_x$ phase. In total 17 such powder patterns were collected during 2.5 days.

Three phases were observed over the whole deuterium concentration range: the D-free alloy $ErCo_3$ and the deuterides β- and γ-$ErCo_3D_x$. The corresponding two-phase regions were clearly visible. For structure refinements the models as derived from the previous neutron and X-ray diffraction experiments were used. Diffraction peaks originating from the sample holder were modelled by using 5 parameters. For each $ErCo_3D_x$ phase 1 scale factor, 2 cell

Table 3
Atomic coordinates, occupancies and thermal displacements in β- and γ-$ErCo_3D_x$, from NPD and synchrotron powder diffraction (space group R-3m)

Atom	Wyckoff site	Occ.	x	y	z	$U_{eq/iso}$, Å^2	U_{11}, Å^2	U_{33}, Å^2
β-$ErCo_3D_x$ (sample No. 1), synchrotron powder diffraction: $a = 4.98638(2)$, $c = 26.0300(3)$Å, $c/a \sim 5.22$, $V = 560.501(6)$ Å^3, $R_B = 0.037$, $R_F = 0.035$, $\chi^2 = 3.72$, $R_p = 0.042$, $R_{wp} = 0.056$, 609 "independent" reflections, 184 "effective" (accounting resolution [11]) reflections.								
Er1	3*a*	1	0	0	0	0.0027(7)	0.0021(6)	0.0039(8)
Er2	6*c*	1	0	0	0.13156(3)	0.0090(6)	0.0037(5)	0.0194(7)
Co1	3*b*	1	0	0	1/2	0.0090(18)	0.0082(18)	0.0106(19)
Co2	6*c*	1	0	0	0.33298(7)	0.0068(12)	0.0095(12)	0.0015(13)
Co3	18*h*	1	0.49842(15)	$-x$	0.07501(4)	0.0023(3)		
β-$ErCo_3D_{1.37(1)}$ (sample No. 2), neutron powder diffraction: $a = 4.98731(13)$, $c = 26.0572(14)$ Å, $c/a \sim 5.22$, $V = 561.30(4)$ Å^3, $R_B = 0.022$, $R_F = 0.018$, $\chi^2 = 1.68$, $R_p = 0.013$, $R_{wp} = 0.016$, 464 "independent" reflections, 142 "effective" reflections.								
Er1	3*a*	1	0	0	0	0.0107(14)	0.0098(10)	0.012(2)
Er2	6*c*	1	0	0	0.13156(9)	0.0162(12)	0.0107(9)	0.0271(17)
Co1	3*b*	1	0	0	1/2	0.014(4)	0.018(4)	0.007(4)
Co2	6*c*	1	0	0	0.3327(3)	0.019(3)	0.024(3)	0.009(3)
Co3	18*h*	1	0.4988(6)	$-x$	0.07445(12)	0.0127(5)		
D1	36*i*	0.315(2)	0.4747(12)	0.4700(12)	0.13754(10)	0.0205(8)		
D2	6*c*	0.164(6)	0	0	0.2204(7)	0.0205(8)		
γ-$ErCo_3D_x$ (sample No. 3), freshly charged with 20 bar of D_2, synchrotron powder diffraction: $a = 5.22488(3)$, $c = 26.12214(19)$ Å, $c/a \sim 5.00$, $V = 617.579(6)$ Å^3, $R_B = 0.027$, $R_F = 0.030$, $\chi^2 = 1.65$, $R_p = 0.040$, $R_{wp} = 0.049$, 426 "independent" reflections, 155 "effective" reflections.								
Er1	3*a*	1	0	0	0	0.0262(9)	0.0306(9)	0.0173(9)
Er2	6*c*	1	0	0	0.13442(2)	0.0135(6)	0.0131(5)	0.0143(6)
Co1	3*b*	1	0	0	1/2	0.0074(17)	0.0089(17)	0.0045(18)
Co2	6*c*	1	0	0	0.33243(7)	0.0429(18)	0.0625(20)	0.0035(15)
Co3	18*h*	1	0.49214(14)	$-x$	0.07653(4)	0.0070(3)		
γ-$ErCo_3D_{3.71(6)}$ (sample No. 4), neutron powder diffraction: $a = 5.2218(3)$, $c = 26.0456(18)$ Å, $c/a \sim 4.99$, $V = 615.05(7)$ Å^3, $R_B = 0.034$, $R_F = 0.028$, $\chi^2 = 1.75$, $R_p = 0.010$, $R_{wp} = 0.013$, 220 "independent" reflections, 108 "effective" reflections.								
Er1	3*a*	1	0	0	0	0.023(3)	0.030(3)	0.011(3)
Er2	6*c*	1	0	0	0.13416(12)	0.016(2)	0.0119(16)	0.020(3)
Co1	3*b*	1	0	0	1/2	0.0014(18)		
Co2	6*c*	1	0	0	0.3342(5)	0.053(6)	0.074(10)	0.0089(7)
Co3	18*h*	1	0.4933(7)	$-x$	0.07671(18)	0.0136(8)		
D1	36*i*	0.366(3)	0.4536(9)	0.4544(9)	0.13885(12)	0.0177(6)		
D3	9*e*	0.348(7)	1/2	0	0	0.0177(6)		
D4	18*h*	0.50(2)	0.8427(9)	$-x$	0.0621(4)	0.0177(6)		
D5	18*h*	0.33(2)	0.8532(10)	$-x$	0.0760(6)	0.0177(6)		
D6	18*h*	0.124(5)	0.7710(17)	$-x$	0.1177(7)	0.0177(6)		

and 2–4 profile parameters were refined. The background was approximated by a polynomial with 5 refined coefficients. Deuterium atom occupancies were independently refined for the β-phase (two D sites), while for the γ-phase the occupancies of the D-atom sites were those of the HRPT data and scaled by one refined parameter. A summary of results is presented in Table 4.

3. Results and discussion

3.1. Phase relations

The in situ NPD experiment on the $ErCo_3$–deuterium system at 60 °C and 0–16 bar revealed the presence of three phases: an α-phase (alloy) at deuterium content below the detection limit of the experiment, a β-phase at intermediate deuterium contents, and a deuterium-rich γ-phase. As shown in Table 4, the β-$ErCo_3D_x$ phase extends over the compositional range $x = 1.07-1.38$ which differs slightly from that reported previously under similar conditions ($x = 1.15-1.65$ at 0.15–1.5 bar and 60 °C [8]). The cell parameters of the β-phase cover the ranges $a = 4.984(2)-4.991(1)$, $c = 25.46(2)-26.032(9)$ Å, $V = 547.7(4)-561.7(2)$ Å^3. Compared to the alloy, a is nearly unchanged (0.1–0.3% expansion), while c increases by 5.1–7.5% as the deuterium content increases from 1.07 to 1.38 D/f.u. Unlike the nickel-based $ErNi_3$–D_2 system [1], there exist no distinct β_1- and β_2-phases but only one single

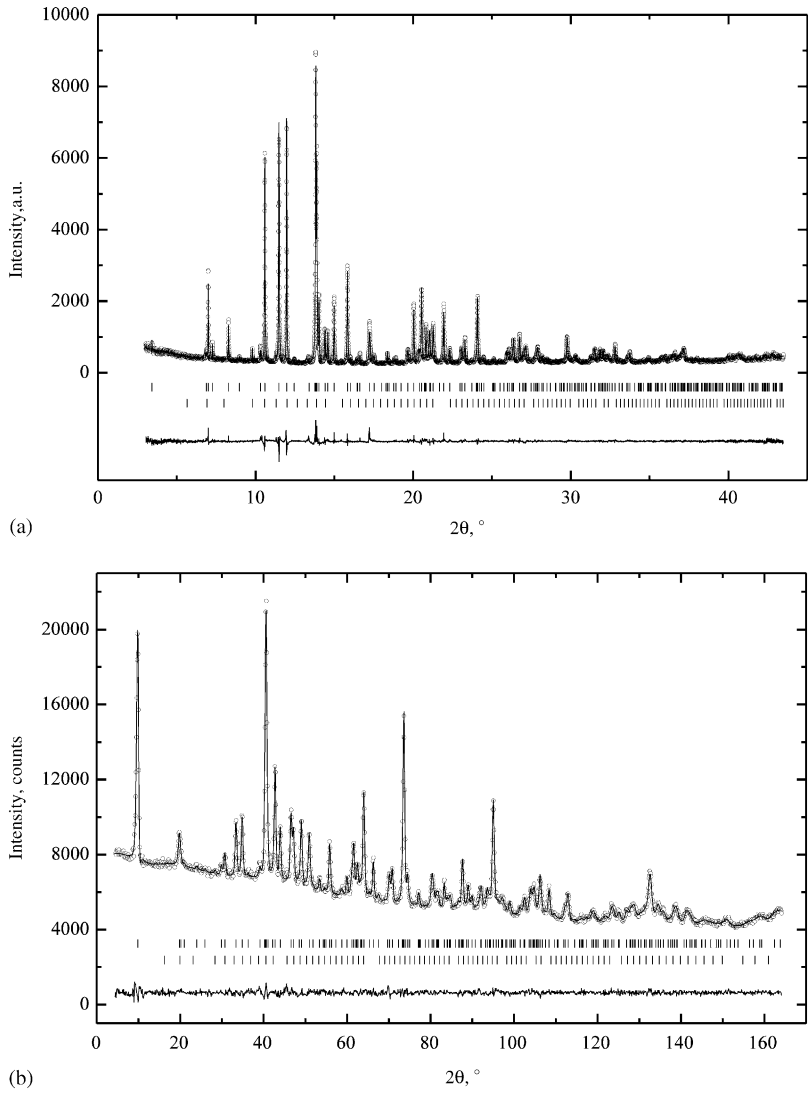

Fig. 1. Observed (points), calculated (line) and difference (bottom line) synchrotron (a) and neutron (b) diffraction patterns for the β-$ErCo_3D_x$ samples; bottom row of vertical bars indicate Bragg positions of the impurity phase (Er_2O_3, ~1 wt%).

β-phase. The γ-$ErCo_3D_x$ phase extends over the compositional range $x = 3.7-4.3$ for which the upper value refers to the experiment at 16 bar D_2 pressure and 25 °C. As for the β-phase the previously reported compositions ($x = 3.3-3.9$ at 60 °C and 1.5–10 bar pressure [8]) appear to be somewhat underestimated. The cell parameters cover the ranges $a = 5.211(2)-5.2318(8)$, $c = 26.07(2)-26.134(7)$, $V = 613.2(5)-619.5(2)$ Å^3. Compared to the alloy, a increases by 4.8–5.2% and c by 7.5–8.2%. As can be seen from Table 3 the cell parameters as derived from the ex situ diffraction experiments correspond closely to those of the fully saturated β-phase ($x = 1.37$) and the D-poor limit of the γ-phase ($x = 3.71$). Thus the cell parameters and deuterium contents as derived independently from in situ and high-resolution ex situ NPD data are consistent with each other.

The phase transitions can be studied most conveniently from plots of the axial ratio c/a or refined D content/f.u. versus the rhombohedral cell volume. As shown in Fig. 3 both plots show relatively good correlations. The c/a ratio increases abruptly between the alloy and the β-phase and then continues to increase at a similar rate within the homogeneity range of the β-phase (Fig. 3a). Upon transition to the γ-phase c/a decreases abruptly and then increases at a much smaller rate within the γ-phase. On the other hand, the refined deuterium content increases more-or-less continuously with cell volume (Fig. 3b). The smaller slope for the β-phase indicates that deuterium in β-$ErCo_3D_x$ occupies a slightly bigger volume (2.9–3.4 Å^3 per D-atom) than in γ-$ErCo_3D_x$ (2.6–2.8 Å^3 per D-atom). These correlations suggest that the deuterium content of the various $ErCo_3D_x$ phases can be estimated to a relatively high precision solely from c/a ratios determined from X-ray powder diffraction.

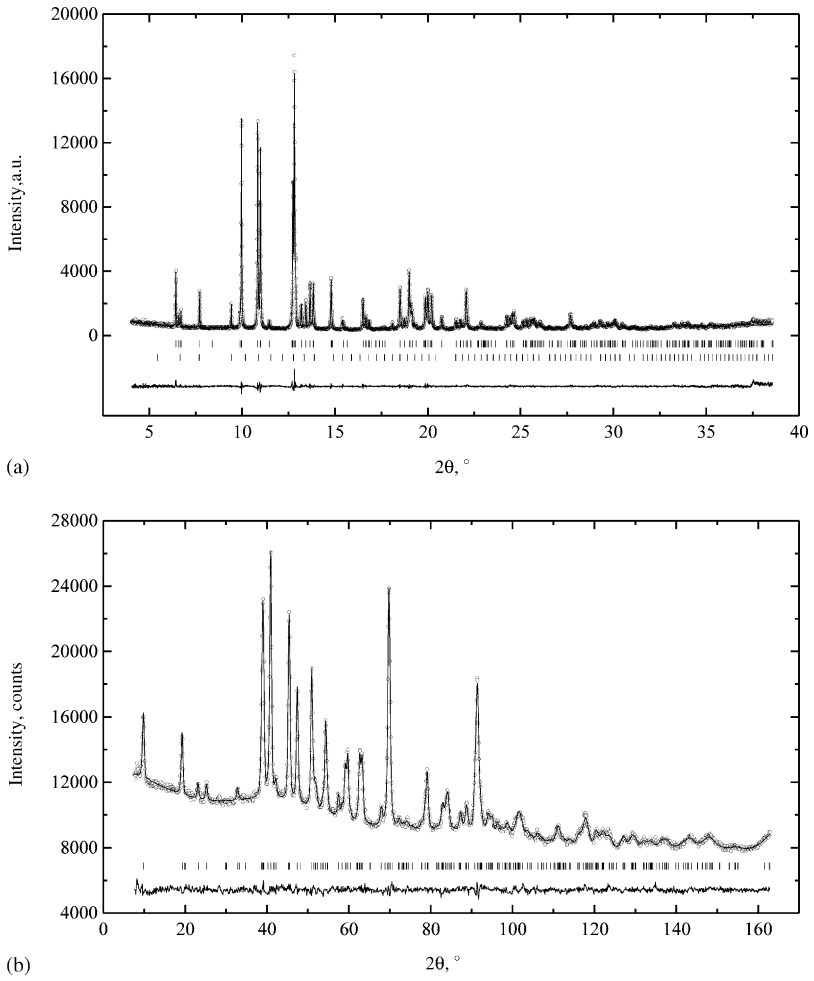

Fig. 2. Observed (points), calculated (line) and difference (bottom line) synchrotron (a) and neutron (b) diffraction patterns for the γ-$ErCo_3D_x$ samples; bottom row of vertical bars indicate Bragg positions of the secondary phase (Er_2O_3, ~1 wt%).

3.2. Structures of β- and γ-$ErCo_3D_x$

Both deuteride phases crystallize with the same symmetry as their parent alloy (space group R-3m). β-$ErCo_3D_{1.37}$ displays two disordered D-atom sites located in the AB_2 building block (D1, D2), while γ-$ErCo_3D_{3.71}$ displays five D-atom sites (D1, D3–D5) of which two (D4 and D5) are located within the same interstice, while one of the β-phase sites (D2) is not occupied. A comparison between the crystal structures of β-$ErCo_3D_{1.37}$ and γ-$ErCo_3D_{3.71}$ is shown in Fig. 4, and the metal atom environments and occupancies of their D-atom sites are summarized and compared with those of other Co and Ni-based $PuNi_3$-type deuterides in Table 5. The various D-atom sites can be discussed as follows (for structural drawings of the various interstitial sites see [12]).

Site D1 (called 36i_1 in [13]) is essentially the same as that (called 18h_7 in [13]) in cobalt-based YCo_3D_x [7] and nickel-based $ErNi_3D_x$ [1] and $HoNi_3D_x$ [2]. Unconstrained refinements of its coordinates showed a slight preference for the general position 36i_1 over the special position 18h_7. The D1–D1 distance is ~0.28 Å in the β-phase and ~0.48 Å in the γ-phase. Within the solid solution range of β-$ErCo_3D_x$ its occupancy grows continuously from 1.0 to 1.3 D/f.u. These values compare well with the 1.32 D/f.u. in β_1-$YCo_3D_{1.32}$, but are significantly lower than the 2.00 D/f.u. in β_2-$YCo_3D_{2.00}$ for which a fully occupied site 18h_7 was found [7]. In γ-$ErCo_3D_{3.7}$ the occupancy of D1 increases to 1.46 D/f.u. On the other hand, this site accommodates only a maximum of ~1 D/f.u. (50% occupancy of 18h_7 site) in nickel-based γ-$ErNi_3D_{3.75}$. However, the latter compound crystallizes with lower symmetry which means that its D1 site have only half the multiplicity (9b in space group R3m) and is fully occupied. In the present $ErCo_3D_x$ there is no experimental evidence for such a symmetry lowering.

Site D2 (called 6c_1 in [13]) is partially occupied (16.4%) in β-$ErCo_3D_x$, and empty in the γ-phase. Due to the short D1–D2 contacts, the sum of occupancies of the 18h_7 and 6c_1 sites cannot be higher than 100%. In the β_1- and β_2-deuterides of the nickel-based $ErNi_3D_x$ and $HoNi_3D_x$ the non-centrosymmetrical analogue of this site (3a in space group R-3m) is fully occupied, which corresponds to a three times larger number of D-atoms on the 6c_1 site than

Table 4
Results of the in situ NPD upon deuterium absorption by $ErCo_3$

No.	Conditions	Phase (refined D-content)	Phase content, %	a, Å	c, Å	V, Å^3
1	Vacuum, 60 °C	$ErCo_3$	100	4.978(2)	24.227(18)	520.0(5)
2		$ErCo_3$	28	4.979(4)	24.25(3)	520.8(9)
		β-$ErCo_3D_{1.07(4)}$	72	4.9837(16)	25.463(17)	547.7(4)
3	Small portions of D_2 gas were let in	β-$ErCo_3D_{1.14(3)}$	100	4.9859(9)	25.626(10)	551.7(2)
4		β-$ErCo_3D_{1.20(3)}$	100	4.9871(8)	25.690(9)	553.3(2)
5	D_2 pressure ~0.1–1 bar	β-$ErCo_3D_{1.27(3)}$	100	4.9894(9)	25.834(9)	557.0(2)
6		β-$ErCo_3D_{1.36(3)}$	100	4.9910(9)	25.963(8)	560.1(2)
7	60 °C	β-$ErCo_3D_{1.38(4)}$	100	4.9910(9)	26.018(8)	561.3(2)
8		β-$ErCo_3D_{1.38(3)}$	92	4.9914(10)	26.032(9)	561.7(2)
		γ-$ErCo_3D_{3.71}$	8	5.217(9)	26.21(9)	617(3)
9	2.5 bar D_2, 60 °C	β-$ErCo_3D_{1.37(3)}$	84	4.9920(10)	26.017(9)	561.5(3)
		γ-$ErCo_3D_{3.71}$	16	5.213(5)	26.16(4)	616(1)
10	2.5 bar D_2, 60 °C	β-$ErCo_3D_{1.35(4)}$	72	4.9924(13)	25.997(11)	561.2(3)
		γ-$ErCo_3D_{3.71}$	28	5.210(3)	26.14(3)	614.5(8)
11	3.0 bar D_2, 60 °C	β-$ErCo_3D_{1.35}$	29	4.996(4)	25.94(3)	560.7(10)
		γ-$ErCo_3D_{3.71}$	71	5.2113(16)	26.074(18)	613.2(5)
12	4.0 bar D_2, 60 °C	γ-$ErCo_3D_{3.84(6)}$	100	5.2189(8)	26.044(7)	614.3(2)
13	6 bar D_2, 60 °C	γ-$ErCo_3D_{3.91(6)}$	100	5.2250(8)	26.071(7)	616.4(2)
14	9 bar D_2, 60 °C	γ-$ErCo_3D_{4.13(5)}$	100	5.2277(8)	26.098(7)	617.7(2)
15	12 bar D_2, 60 °C	γ-$ErCo_3D_{4.17(5)}$	100	5.2298(7)	26.115(6)	618.6(2)
16	16 bar D_2, 60 °C	γ-$ErCo_3D_{4.20(6)}$	100	5.2318(8)	26.134(7)	619.5(2)
17	16 bar D_2, 25 °C	γ-$ErCo_3D_{4.30(5)}$	100	5.2356(7)	26.202(6)	622.0(2)

in β-$ErCo_3D_{1.37}$. A depopulated $6c_1$ site was already found in the γ-phase of the nickel analogue $ErNi_3D_{3.75}$ [1] and in the deuteride phases of cobalt-based YCo_3D_x [7]. In the latter, the D1 site ($18h_7$) in β_2- and γ-YCo_3D_x are completely filled and thus prevent the $6c_1$ sites from becoming occupied. In the present β-$ErCo_3D_x$ phase in situ NPD showed that the occupancy of D_2 remains nearly constant (0.1 D/f.u.).

Site D3 ($9e$) becomes occupied only in the γ-phase. Its position is close to that of the partially occupied $18h_8$ site (nomenclature according to [13]) in the nickel-based analogues, being situated at only ~0.45 Å from, and half-way between neighbouring $18h_8$–$18h_8$ sites. The number of D-atoms on site $9e$ corresponds to 0.35 D/f.u., which compares well with the 0.27 and 0.23 D/f.u. in β_2-$ErNi_3D_{1.97}$ and β_2-$HoNi_3D_{1.8}$, respectively, but it is considerably smaller than the 0.74 D/f.u. in γ-$ErNi_3D_{3.75}$.

Sites D4 and D5 (called $18h_2$ in [13]) are located within the same metal interstice and are occupied only in the γ-phase. They are situated just ~0.3 Å apart and their total occupancy is ~88%, which is close to the 84% as reported before for the single $18h_2$ site in γ-$ErCo_3D_{3.4}$ [6].

Site D6 ($18h_3$) has been reported before only in the nickel analogue γ-$ErNi_3D_{3.75}$ [1]. In the earlier structure determination of γ-$ErCo_3D_{3.4}$ [6] this position was not identified and here we report only a low occupancy of ~12%. Since there are short exclusive D–D contacts between sites D4 (D5) and D6, their total occupancy cannot be higher than 100%. Indeed, both in γ-$ErCo_3D_{3.7}$ and γ-$ErNi_3D_{3.75}$ this sum is equal to 100% within two standard uncertainties.

As expected, the deuterium-induced cell expansion leads to a considerable elongation of some Co–Co bonds (see Table 6). The transition from the alloy to the β-deuteride, for example, leads to an expansion of the AB_2 building block that increases the Co1–Co3 distances by ~0.25 Å, while the other Co–Co distances remain nearly unaffected. This elongation is consistent with the occupation of D1 bridging the Co1–Co3 bond. Upon the formation of the γ-deuteride the cell expands mainly in the basal plane, thus shortening slightly the Co1–Co3 bonds. At the same time the Co2–Co3 bonds within the AB_5 block are elongated by ~0.08 Å, on the average. The main changes, however, concern the Co3–Co3 bonds: two out of four formed by each Co3 atom elongate by more than 0.2 Å due to the bridging D4, D5, and D6 atoms. The corresponding elongation of Ni–Ni bonds in RNi_3D_x (R = Er, Ho) [1,2] is of a similar nature except that the Ni1–Ni3 bonds in the AB_2 building block show a considerable asymmetry due to the hydrogen-induced loss of inversion symmetry. As expected, only those Ni–Ni bonds are elongated that are bridged by D-atoms.

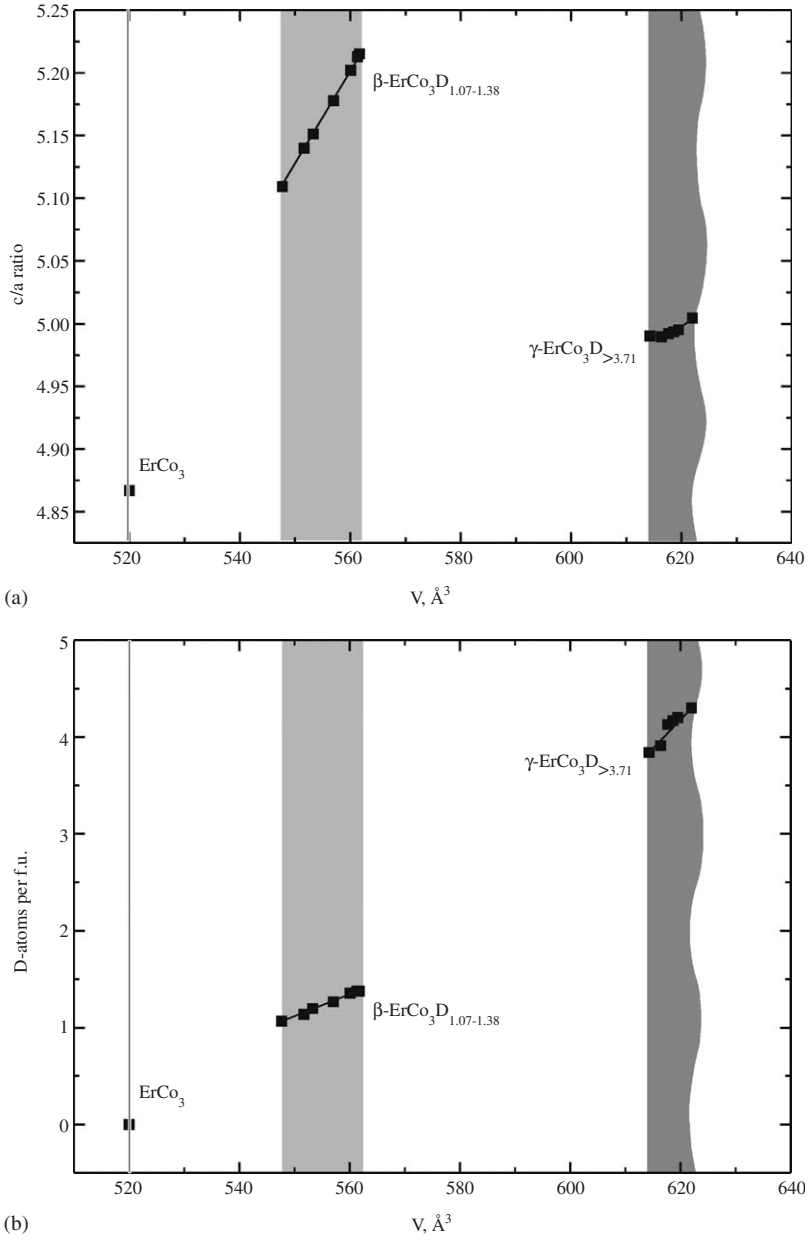

Fig. 3. The c/a ratio (a) and refined deuterium content (b) versus the unit cell volume for the rhombohedral $ErCo_3D_x$ phases, as determined from in situ NPD at 60 °C (data from Table 4 only from single-phase samples).

Finally, deuteration of $ErCo_3$ leads to an expansion of the anisotropic displacement ellipsoid of Co2 in the basal plane for both the β- and γ-phases. This observation is made with both synchrotron and neutron diffraction data. The anisotropy is more pronounced for the γ-phase, the root-mean-square displacement in the basal plane (0.27 Å) being three times bigger than along the c-axis (0.09 Å). A possible reason for this could be the close proximity of the partially occupied D3 site (occupancy ~35%) which favours local displacements of Co2 atoms. Another reason could be a local ordering of deuterium atoms. As was shown before [1,2] such an ordering occurs in the nickel compounds and is accompanied by a symmetry lowering of the metal matrix. Cell distortions at room and low temperature were observed in $PrCo_3H_{4.8}$ [5] and γ-YCo_3H_x [14].

3.3. Transition metal environment and directional Co–D bonding

In β-$ErCo_3D_{1.37}$ the average number of deuterium ligands around cobalt is ~3.8 for Co1 (AB_2 block) and ~0.8 for Co3 (AB_2/AB_5 boundary). The Co2 atom (AB_5 block) has no nearest D-neighbours. Upon transition to γ-$ErCo_3D_{3.7}$ the D-atoms also fill the AB_5 block and the average number of deuterium ligands increases to ~4.4 for Co1, ~1.0 for Co2 and ~3.0 for Co3. The Co–D distances remain virtually unchanged upon this transition (Table 6).

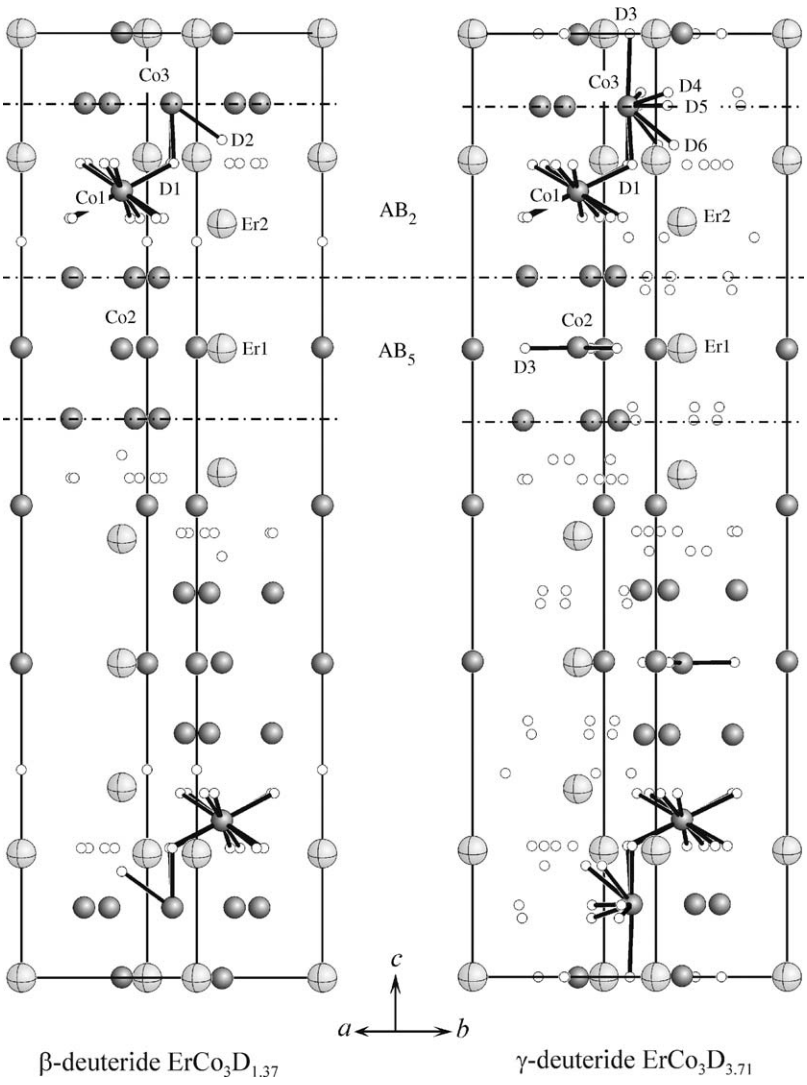

Fig. 4. Crystal structure of rhombohedral β-$ErCo_3D_{1.37}$ and γ-$ErCo_3D_{3.71}$; D-atom environments around Co atoms are highlighted.

The D-atom environments around the three Co sites in γ-$ErCo_3D_{3.71}$ are shown in Fig. 5. Co1 is surrounded by the split-atom site D1 ($36i_1$, see Section 3.1) in a distorted octahedral configuration, of which four out of six apices, on the average, are occupied by D-atoms. Locally, distorted square-planar or saddle-like [CoD_4] configurations are possible. Co2 is surrounded by one D-atom on the average (D3, 35% occupied) in a disordered trigonal planar configuration. Co3 has a complex disordered D-atom environment with an average of three D-ligands.

3.4. Comparison between nickel and cobalt analogues

Among the known RT_3–D_2 systems structure data are available for comparison for the two cobalt-based systems YCo_3D_x and $ErCo_3D_4$, and the two nickel-based systems $ErNi_3D_x$ and $HoNi_3D_x$. As shown in Table 5, the main differences between the Co and Ni-based systems concern their structural symmetry and the D-atom environment of some T metal sites. While the Co-based deuterides crystallize with the centrosymmetric structure of their corresponding alloys (space group R-3m), the Ni-containing deuterides display a loss of inversion symmetry (space group R3m). This loss is reflected in the D-atom environment around the T metal atom within the AB_2 building blocks. In the cobalt compounds Co1 (point group -3m) is surrounded by an average of 3.8 (β-$ErCo_3D_{1.37}$), 4 (β_1-$YCo_3D_{1.24}$), 4.4 (γ-$ErCo_3D_{3.7}$) and 6 D-atoms (β_2-$YCo_3D_{2.0}$, γ-$YCo_3D_{4.6}$) in partly disordered, distorted octahedral configurations, while in the nickel compounds Ni1 (point group symmetry 3m) is surrounded by ~3 (β_1- and β_2-RNi_3D_x, R = Er, Ho) and ~4 (γ-$ErNi_3D_{3.7}$) D-atoms in disordered trigonal (pyramidal) and tetrahedral configurations, respectively. In view of the similar atomic radii of Ni and Co these results indicate that the hydrogen distributions in this homologous series depend on the nature of the transition element rather than on geometric factors. This observation has already been made

Table 5
Deuterium occupied interstitials in $PuNi_3$-type structures

Interstitial, notation of Burnasheva [13] (sp. gr. *R*-3*m*)	D-atom environment	β_1-$YCo_3D_{1.24}$ (*R*-3*m*)	β_2-$YCo_3D_{2.0}$ (*R*-3*m*)	γ-$YCo_3D_{4.6}$ (*R*-3*m*)	β-$ErCo_3D_{1.37}$ (*R*-3*m*)	γ-$ErCo_3D_{3.7}$ (*R*-3*m*)	γ-$ErCo_3D_{3.4}$ (*R*-3*m*)	β_1-$ErNi_3D_{1.23}$ (*R*3*m*)	β_2-$ErNi_3D_{1.97}$ (*R*3*m*)	γ-$ErNi_3D_{3.75}$ (*R*3*m*)	β-$HoNi_3D_{1.8}$ (*R*-3*m*)	β_1-$HoNi_3D_{1.3}$ (*R*3*m*)	β_2-$HoNi_3D_{1.8}$ (*R*3*m*)
		[7]	[7]	[7]	This work	This work	[6][b]	[1]	[1]	[1]	[13][c]	[2]	[2]
$18h_7$ (AB_2 unit)[a] close to $36i_1$	Trig. bipyr. RT_2 base + 2*R*	66%	100%	100%	63.0(4)% $36i_1$	73.2(6)% $36i_1$	70(1)%	92(1)%	115(3)%	77(4)%	0%	95(2)%	102(3)%
$18h_2$ (AB_2/AB_5 boundary)	Tetrahedron R_2T_2			100%		50(2)% 33(2)%	84(2)%		30(2)%	96(4)% 60(4)%			25(2)%
$18h_8$ (AB_5 unit)[d] close to 9*e* or $36i_2$	Trig. bipyr. T_3 base + 2*R*			32%		17.4(3)% 9*e*	16(2)% $36i_2$		27(2)%	72(4)%			23(2)%
$18h_1$ (AB_2/AB_5 boundary)	Tetrahedron R_2T_2										64%		
$6c_1$ (AB_2 unit)	Tetrahedron RT_3				16.4(6)			95(2)%	77(4)%		78%	95(3)%	108(4)%
$18h_3$ (AB_2 unit)	Tetrahedron R_2T_2					12.4(5)%	0%			37(3)%			
$6c_3$ (AB_2 unit)	Tetrahedron T_4									98(6)%			

[a]Trigonal-bipyramidal site $18h_7$ situated between two tetrahedral $36i_1$ (1.2 Å apart) was introduced by Liu [7]. Although a partially filled $18h_7$ site has been identified earlier, no identifier was attributed [6].

[b]Revised in this work.

[c]Resived in [2].

[d]Site $18h_8$ is situated between two $36i_2$ sites, distance $36i_2$–$36i_2$ is 1.1 Å. 9*e* site is situated between two $18h_8$ sites, distance $18h_8$–$18h_8$ is 0.9 Å. While 9*e* site is exactly in the centre of the R_2T_4 octahedron, the $18h_8$ and $36i_2$ sites are displaced from the centre towards an apex (trigonal-pyramidal $18h_8$) or a face (tetrahedral $36i_2$). Although $36i_2$ and 9*e* interstitials were mentioned by Burnasheva [13], $18h_8$ was not. Partially filled $18h_8$ interstitial was identified by Liu [7], however no identifier was attributed, $36i_2$ notation was used instead.

Table 6
Shortest Co–Co and Co–D distances (Å) in $ErCo_3$ and its deuterides

	$ErCo_3$	β-$ErCo_3D_x$, $x = 1.37$		γ-$ErCo_3D_x$, $x = 3.71$	
	X-rays	NPD	Synchr.	NPD	Synchr.
Co1–6Co3	2.539(3)	2.796(3)	2.780(1)	2.754(4)	2.759(1)
Co1–12D1		1.651(5)		1.686(4)	
Co2–3Co3	2.421(4)	2.409(7)	2.425(3)	2.449(11)	2.481(2)
Co2–3Co3	2.448(4)	2.422(3)	2.426(2)	2.557(11)	2.529(2)
Co2–3D3				1.5076(2)	
Co3–2Co3	2.445(3)	2.476(4)	2.470(1)	2.507(5)	2.489(1)
Co3–2Co3	2.533(3)	2.511(5)	2.517(1)	2.715(5)	2.736(1)
Co3–2D1		1.650(4)		1.637(6)	
Co3–D2		1.76(1)			
Co3–D3				1.999(5)	
Co3–2D4				1.625(6)	
Co3–2D5				1.631(7)	
Co3–2D6				1.74(1)	

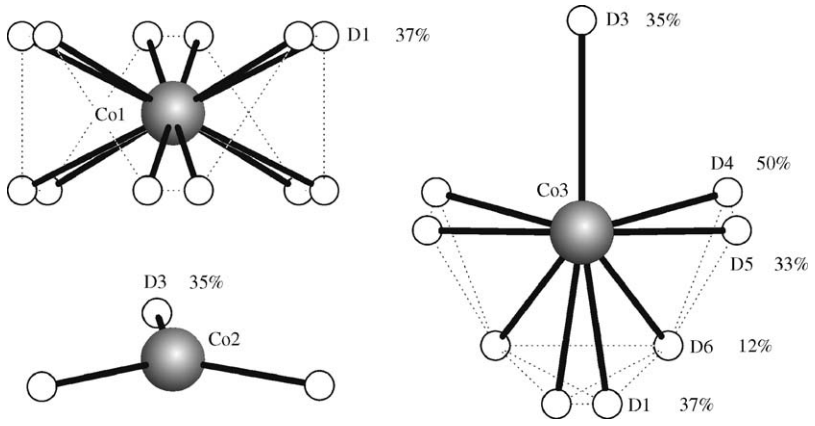

Fig. 5. D-atom environments around Co atoms in the γ-$ErCo_3D_{3.71}$. D–D distances shorter than 2 Å are marked by dashed lines, D-sites' occupancies are indicated.

while studying the so-called "complex" transition metal hydrides (for reviews see [15]). The *T* metals in this class of (non-metallic) hydrides form hydride complexes that display preferred geometric and electronic configurations, such as the nickel-based tetrahedral 18-electron $[NiH_4]^{4-}$ complexes in Mg_2NiH_4 and $LaMg_2NiH_7$, and the cobalt-based square pyramidal 18-electron $[CoH_5]^{4-}$ complexes in Mg_2CoH_5, $Mg_6Co_2H_{11}$ and $Ca_4Mg_4Co_3H_{19}$. In analogy with the present (metallic) hydrides one can speculate that directional metal–hydrogen bonding effects also prevail in "interstitial" hydrides. In other words, the interstitial concept which is based exclusively on geometrical arguments should be revised in order to explain structural details in the vicinity of the *T* metals.

Acknowledgments

We thank Prof. D.K. Ross (Salford) for providing structure data on $YCo_3H(D)_x$ prior to publication. This work was supported by the Swiss National Science Foundation and the Swiss Federal Office of Energy. It has been partially performed at the Swiss Spallation Neutron Source SINQ, Paul Scherrer Institute, Villigen, Switzerland, and the Swiss–Norwegian Beamline, ESRF, Grenoble, France.

References

[1] Y. Filinchuk, K. Yvon, J. Alloys Compds. 404–406 (2005) 89–94.
[2] Y. Filinchuk, D. Sheptyakov, K. Yvon, J. Alloys Compds. (2005), in press; http://dx.doi.org/10.1016/j.jallcom.2005.06.068
[3] M. Latroche, V. Paul-Boncour, A. Percheron-Guégan, J. Solid State Chem. 177 (2004) 2542–2549.
[4] C.A. Bechman, A. Goudy, T. Takeshita, W.E. Wallace, R.S. Craig, Inorg. Chem. 15 (1976) 2184–2187.
[5] V.V. Burnasheva, V.V. Klimeshin, V.A. Yartys', K.N. Semenenko, Inorg. Mater., transl. from Izv. Akad. Nauk. SSSR, Neorg. Mater. 15 (1979) 627–632.
[6] M.I. Bartashevich, A.N. Pirogov, V.I. Voronin, T. Goto, M. Yamaguchi, I. Yamamoto, J. Alloys Compds. 231 (1995) 104–107.

[7] J. Liu, P.A. Georgiev, D.K. Ross, M. Roberts, K.A. Andersen, M. Telling, D. Fort (2005), unpublished.
[8] H.A. Kierstead, J. Less-Common Met. 78 (1981) 61–68.
[9] D.M. Gualtieri, W.E. Wallace, J. Less-Common Met. 61 (1978) 261–264.
[10] R.M. Donohue, A.J. Goudy, Inorg. Chem. 30 (1991) 800–802.
[11] J. Rodriguez-Carvajal, FULLPROF SUITE, LLB Sacley & LCSIM Rennes, France, 2003.
[12] M. Latroche, A. Percheron-Guégan, J. Alloys Compds. 356–357 (2003) 461–468.
[13] V.V. Burnasheva, V.A. Yartys', S.P. Solov'ev, N.V. Fadeeva, K.N. Semenenko, Sov. Phys. Crystallogr. 27 (1982) 409.
[14] M. Bartashevich, T. Goto, M. Yamaguchi, I. Yamamoto, A.V. Andreev, Solid State Commun. 82 (1992) 201–204.
[15] K. Yvon, Metal Hydrides: Transition Metal Hydride Complexes. Encycl. Mater.: Sci. Technol., vols. 1–9, Elsevier Ltd, Amsterdam, 2004;
K. Yvon, G. Renaudin, Hydrides: Solid State Transition Metal Complexes. Encycl. Inorg. Chem., second ed, Wiley, New York, ISBN 0-470-86078-2, 2005.